

Emplacement of the Fogo Island Batholith, Newfoundland

K.L. CURRIE*

Geological Survey of Canada, 601 Booth Street, Ottawa, ON K1A 0E8

* Correspondence address: 9 Tiverton Drive, Nepean, ON K2E 6L4

Date received: July 28, 2003 ¶ *Date accepted: October 11, 2003*

ABSTRACT

The Siluro-Devonian Fogo Island Batholith is a high-level, bimodal, sill-like unit about 7 km thick, intruded by a slightly younger, heterogeneous mafic unit. Stratigraphic evidence suggests emplacement of the batholith by raising of the roof without strong deformation of the host rocks. Large composite gabbro-microgranite dykes below the sill, intruded along axial planar cleavage, probably served as feeders. The upper 3–4 km of the sill comprise homogeneous to slightly zoned, coarse, hastingsite-biotite granite. Ignimbrite sheets of similar composition above the sill suggest that the granite was emplaced beneath cover rocks no more than 1 km thick. The lower 3 km of the sill consist of heterogeneous, locally layered, mafic rocks. Metre-scale, non-intrusive sheets of contrasting composition mark the contact between the granitic upper and mafic lower part of the sill. A late influx of mafic magma disrupted older mafic rocks and hybridised with granite, producing complex, heterogeneous “diorite”. The local presence of A-type compositions in the granitic portion of the batholith may reflect diffusion during this process. A model for emplacement of the batholith assumes crustal anatexis above mantle-derived, underplated mafic magma, followed by passive emplacement of composite magma along tensional fractures related to movements on the Dog Bay Line, a dextral terrane boundary. Later movements on this feature controlled emplacement of further batches of magma, and finally tipped the batholith about 25° to the north, producing its present configuration.

RÉSUMÉ

Le Batholithe siluro-dévonien de l'île Fogo forme une unité à l'aspect d'un filon-couche bimodale de niveau élevé et d'environ sept kilomètres d'épaisseur, dans laquelle fait intrusion une unité mafique hétérogène légèrement plus récente. Les observations stratigraphiques laissent supposer une mise en place du batholithe par soulèvement du toit sans déformation marquée des roches hôtes. Des dykes composites de gabbro-rhyolite de fortes dimensions au-dessous du filon-couche, ayant subi une intrusion le long de la schistosité de plan axial, ont probablement servi de voies de passage. Les trois à quatre kilomètres supérieurs du filon-couche sont constitués de granite à hastingsite-biotite grossier allant d'homogène à légèrement zoné. Des couches de tuf consolidé d'une composition semblable au-dessus du filon-couche permettent de supposer que la mise en place du granite s'est faite sous des roches de couverture d'au plus un kilomètre d'épaisseur. Les trois kilomètres inférieurs du filon-couche sont constitués de roches mafiques hétérogènes, localement stratifiées. Des nappes non intrusives de quelques mètres d'une composition différente marquent la zone de contact entre le sommet granitique et la base mafique du filon-couche. Un afflux tardif de magma mafique a perturbé les roches mafiques âgées et a entraîné une hybridation avec le granite, produisant des « diorites » hétérogènes complexes. La présence locale de compositions de type A dans la partie granitique du batholithe pourraient témoigner d'une diffusion au cours de ce processus. Un modèle de mise en place du batholithe suppose une anatexie crustale au-dessus d'un magma mafique reposant sur des plaques et d'origine mantellique, suivie de la mise en place passive de magma composite le long de fractures de tension apparentées à des mouvements survenus le long de la ligne Dog Bay, une ligne de démarcation de terrane dextre. Des mouvements ultérieurs le long de cette ligne ont déterminé la mise en place d'autres mélanges de magma et ont finalement incliné le batholithe d'environ 25 degrés vers le nord, pour produire sa configuration existante.

[Traduit par la rédaction]

INTRODUCTION

Batholith emplacement, by definition, takes place deep within the crust under conditions which are difficult to determine precisely, and even more difficult to scale accurately in experiment or simulation, rendering dubious the applicability of conclusions reached from experimental and modelling stud-

ies. Compare, for example, thermal modelling studies indicating that diapiric ascent of magma in the crust is impossible (Weinberg 1996; Petford 1996) with structural studies of felsic plutons indicating diapir-like emplacement (Sylvester 1964; Paterson and Vernon 1995). However, conditions of emplacement of a batholith can, in favourable cases, be constrained by stratigraphic, structural, and geochemical data. For the Fogo

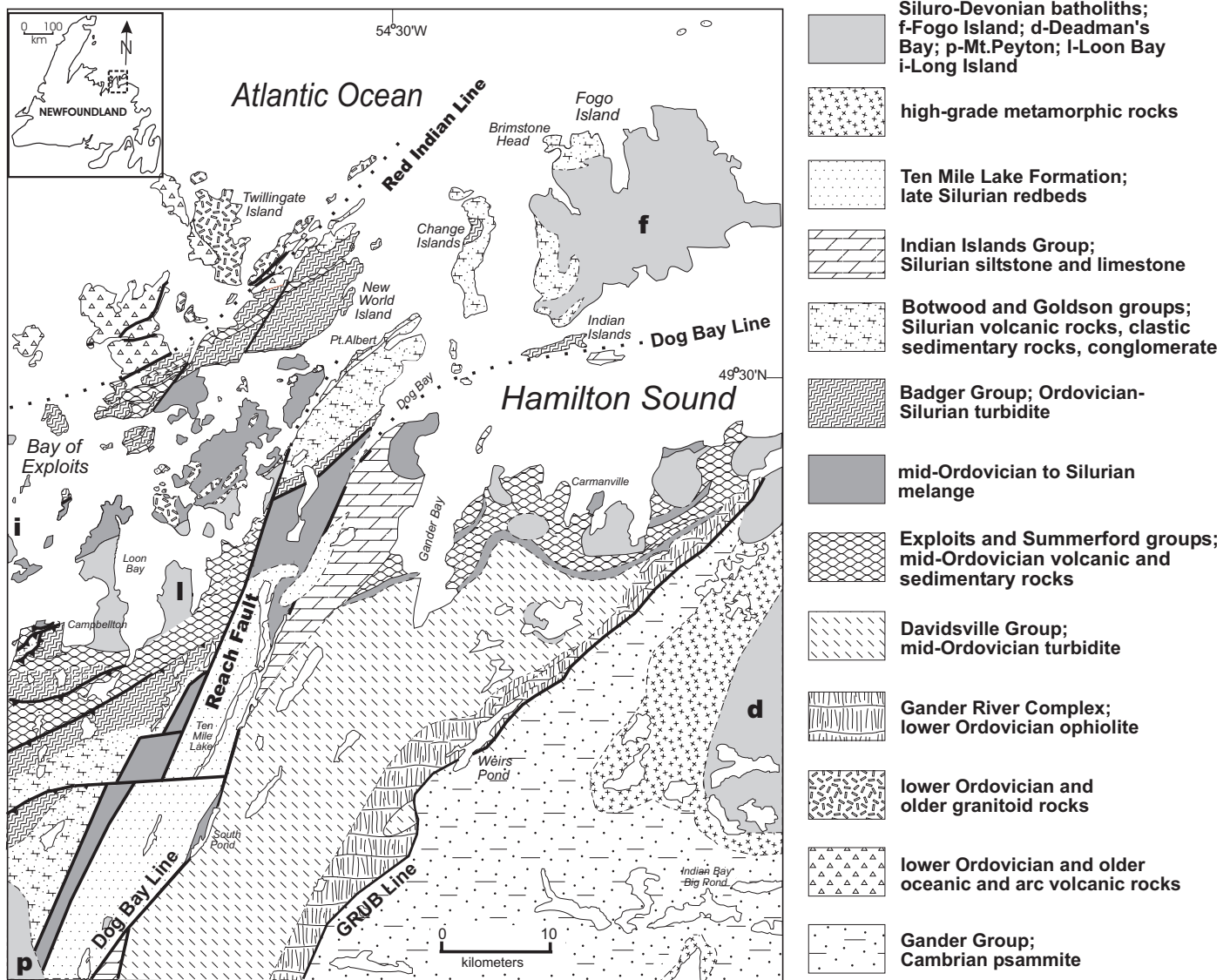


Fig. 1 Regional geological setting of the Fogo Island Batholith (simplified after Currie 1995). The location of the map area is shown by the box on the inset map.

Island Batholith of northeast Newfoundland, these data provide valuable information on the evolution and emplacement of the batholith, including its geometric form and a mechanism of creating sufficient space for emplacement.

GEOLOGICAL SETTING

The Fogo Island Batholith lies within a curved, northeast-trending fault slice dominated by mid-Ordovician to Silurian strata (Fig.1) which underwent polyphase deformation in Silurian time (Karlstrom *et al.* 1982; Currie 1997c). Southwest of Fogo Island, isoclinal, steeply dipping, northeast-trending, northwest-verging structures dominate the outcrop pattern within this slice, but on Fogo Island these folds are open, with limb dips rarely exceeding 40°. The folded strata comprise back-arc volcanogenic rocks of the mid-Ordovician Exploits

Group (O'Brien *et al.* 1997), late Ordovician–early Silurian, westerly-derived, greywacke and conglomerate turbidites of the Late Ordovician–early Silurian Badger Group (Williams *et al.* 1995), and clastic and volcanic rocks of the Silurian Botwood Group (Williams 1972). The Dog Bay Line (Williams *et al.* 1993), a dextral terrane boundary marked by tectonic melange, juxtaposes the Badger and Botwood groups against Silurian limestone and limy coralline siltstone of the Indian Islands Group (Currie 1995). Along the Dog Bay Line, the bimodal Fogo Island Batholith abuts coeval peraluminous anatectic plutons (Currie and Pajari 1981) and the metaluminous early Devonian Deadman's Bay megacrystic pluton (D'Lemos and Holdsworth 1995). Metaluminous Siluro-Devonian bimodal batholiths similar to the Fogo Island Batholith occur between the Dog Bay and Red Indian lines (Mount Peyton, Loon Bay, Long Island), but northwest of the Red Indian Line only sparse Siluro-Devonian salic dykes occur (Elliot *et al.* 1991)

maximum age, and a precise U-Pb zircon age of 422 ± 2 Ma (Ludlow) from a composite dyke cutting the formation on Dog Bay (Elliot *et al.* 1991) provides a minimum age.

A sharp, conformable contact of the Fogo Harbour Formation with the overlying Brimstone Head Formation (Baird 1958) can be traced across northern Fogo Island at the base of a cliff of rhyolite ignimbrite (Currie 1997b). A single metre-scale lens of tuffaceous sandstone resembling the underlying sedimentary section occurs about 60 m above the base of the Brimstone Head Formation at Brimstone Head. On Fogo Island, the Brimstone Head Formation comprises several sheets of densely welded, brown, rhyolite ignimbrite with a foliation marked by elongate pale streaks of less welded material (fiamme). Offshore islands consist of moderately welded crystal tuff and tuff breccia with a few lenses of red, subaerial sandstone up to 10 m thick. The thickness of the formation is unknown, but locally exceeds 1000 m. The composition of the ignimbrite sheets resembles that of salic parts of the Fogo Island Batholith, and the Brimstone Head Formation may represent an erupted portion of the batholith, as suggested by Sandeman and Malpas (1995).

All of the supracrustal rocks on Fogo Island are openly folded about axial planes trending northeast and dipping about 65° to the south. Limb dips rarely exceed 40° , and fold amplitudes vary from a few metres to a few hundred metres. All of the folds exhibit strong axial planar cleavage, a cleavage which is developed on a regional scale, extending tens of kilometres southwest from Fogo Island. An envelope to the folds dips north-northwest at about 25° , so that stratigraphically higher levels are exposed to the north.

Fogo Island Batholith

The Fogo Island Batholith, which underlies 80% of Fogo Island (about 250 km^2) and also appears on small islands up to 8 km offshore to the east and southeast, intrudes the Fogo Harbour Formation. The batholith comprises five distinct lithologies. In order of decreasing age they are (1) agmatite containing blocks of host rock in a coarse-grained igneous matrix, (2) felsite, rhyolite porphyry, and microgranite, (3) layered and massive gabbro, (4) medium- to coarse-grained amphibole-biotite granite, (5) heterogeneous mafic rocks with a generally dioritic to tonalitic matrix containing schliers and blocks ranging from layered gabbro, to monzonitic, syenitic and granitic varieties. In the Tilting Harbour area, Aydin (1995) reported an emplacement age of 422 ± 2 Ma for the amphibole-biotite granite, and 408 ± 2 Ma for agmatitic diorite, consistent with field observations.

Layering in the batholith, commonly present in intermediate to mafic units and locally in granitic units, parallels bedding in nearby sedimentary rocks, and exhibits open folds congruent to those in the host rocks. However, folds in the igneous rocks do not exhibit axial planar cleavage, suggesting that folding in the host rocks pre-dated emplacement of the batholith, at least in part. Both top and bottom contacts of the batholith with the Fogo Harbour Formation can be observed in the western part

of the island, dipping moderately north. These observations indicate a sill-like form for the exposed part of the batholith. Geological mapping shows the batholith to be about 6.5 km thick at its western end increasing to 8 km or more toward the east. The batholith comprises a homogeneous granitic upper part, 3–4 km thick, and a texturally complex intermediate to mafic lower part about 3 km thick.

Minor intrusive bodies related to the batholith occur both above and below the main mass. Dykes related to the batholith tend to strike parallel to bedding in the host rocks, but dip at high angles to bedding, lying in the axial planar cleavage of open folds. Below the body, on the southwest corner of the island, composite dykes up to 60 m thick (Fig. 3) have a core of gabbro up to 20 m thick, commonly plagioclase-porphyrific, with thick rims of porphyry or microgranite chemically indistinguishable from granite of the main body. The contacts between mafic and salic phases are sharp, but lobate, with occasional rounded blobs or streaks of one lithology in the other, indicating some degree of mingling. These distinctive dykes occur up to 20 km from Fogo Island. One gave a precise U-Pb zircon date of 422 ± 2 Ma (Elliot *et al.* 1991), identical to that of the main batholith. In some cases these dykes connect to small microgranite sills or laccoliths. Above the main body near Fogo Harbour, porphyry and microgranite dykes abound, but they lack mafic cores and rarely exceed 15 m in width. Many of these dykes connect to sills up to 10 m thick, with the dyke-sill transition forming prominent rock ridges, possibly due to thickening of the erosionally resistant igneous bodies at this point. Sandeman and Malpas (1995) considered these sills to be ignimbrite sheets, but their intrusive nature is demonstrated by (1) equal and intense hornfelsing of the host on both sides of the sills, and (2) presence of laminated siltstone on both sides with no increase in tuffaceous material.

Agmatite

Although some small-scale contacts of the batholith with its host rocks appear knife-sharp and generally conformable, agmatite (Fig. 4) commonly appears along internal and external contacts of the Fogo Island Batholith and may be up to 100 m thick. Agmatite in contact with the Fogo Harbour Formation consists of 50 to 80% of centimetre to metre-scale hornfelsed blocks of Fogo Harbour Formation in a medium- to coarse-grained matrix which is granitoid along the northern and southwestern margins of the complex, but becomes more tonalitic to the south. Similar agmatite forms a semi-continuous fringe, 10 to 100 m thick, separating granite bodies between Joe Batts Arm and Barr'd Islands. Within the agmatite, the blocks become larger and more coherent with distance from more massive igneous rocks, passing outward into irregularly folded sedimentary rocks with a few granite dykes. Throughout the agmatite, the blocks exhibit a strong preferred orientation, in many examples preserving only slightly disrupted stratigraphy. Within 50 m of the main body, some centimetre-scale beds appear to have melted to thin layers of brownish aphanitic material which locally forms a



Fig. 3 Composite gabbro-rhyolite dyke, quarry west of Little Seldom Cove. The central mafic core of the dyke (dark grey) is 10 m wide with a grain size of 1–2 mm. The microgranite rims, about 20 m wide, are aphanitic. Host rocks, siltstone of the Fogo Harbour Formation, visible to the left of the dyke, dip gently from left to right, perpendicular to the dip of the dyke. The height of the quarry face is about 10 m. Note trees on top for scale.



Fig. 4 Agmatite along the contact of the granite of the Fogo Island Batholith with the Fogo Harbour Formation, north of Island Harbour. Note the well-preserved foliation defined by disrupted beds. The pale grey material surrounding the lenticular fragments is felsite or granophyre, forming about 25% of the volume in this exposure.

selves around blocks. Despite intense hornfelsing and possible local partial melting, new mineral growth was confined to sparse growth of fine biotite, suggesting that cooling took place rapidly enough that thermal equilibrium was never attained.

Felsite, rhyolite porphyry, and microgranite

The upper margin of the granite consists of an almost continuous layer of fine-grained, pink, felsic rock varying from featureless felsite to microgranite with abundant granophyric intergrowth and drusy miarolitic cavities, to rhyolite porphyry that is commonly spherulitic. Similar to identical lithologies occur as sills along the base of the granite where it contacts the mafic phase, and as sills and dykes above and below the batholith. In general felsite occurs close to the coarse-grained granite, whereas microgranite tends to form sills below the batholith, and rhyolite porphyry forms dykes above the batholith. However, there is no sharp division and all these rocks have similar or identical compositions (Appendix 1). A typical feature of all these rocks is presence of thin seams or clots of amphibole and magnetite. These segregations occur erratically in the felsic rocks (which otherwise contain virtually no mafic minerals) and also in hornfelsed country rocks adjacent to them.

Sandeman and Malpas (1995) reported that microgranite sheets cut the batholith, and that coarse-grained granite grades to microgranite. However, contacts between coarse and fine-grained to aphanitic felsic rocks are always sharp where exposed, and where intrusive relations can be determined, the coarse-grained phase invariably cuts the fine-grained one. Chemically no significant differences are present in major element composition between coarse-grained and fine-grained felsic rocks (Appendix 1). Sandeman and Malpas (1995) drew attention to enrichment of the fine-grained rocks in high-field-strength elements and Ga/Al ratio, suggesting an A-type affinity. These tendencies are evident in all the felsic compositions (Fig. 5), and there appear to be no systematic differences in composition between fine-grained rocks and coarse-grained rocks, with the possible exception of slightly lower FeO^*/MgO in the latter.

Gabbro and basalt

Baird (1958) noted the presence of layered mafic rocks around Tilting Harbour and Seldom Come By. The Tilting Layered Suite, which formed the subject of studies by Cawthorn (1978) and Aydin *et al.* (1994), underlies an oval area about 2 by 1.5 km in size, surrounded by hybrid dioritic rocks into which it grades, and by which it is intruded. Centimetre to metre-scale layering faces and dips 35–85° to the north, and consistently pinches out to the southwest. Layers exhibit modal and textural variation, including repeated cycles from websterite bases (cumulate ortho- and clinopyroxene ± olivine) to gabbro or leucogabbro tops (cumulate clinopyroxene and plagioclase). Large poikilitic hornblende and in some cases plagioclase overgrow the cumulates. Local convolute layering

and prominent size and density sorting in some layers suggest deposition from magmatic currents, although much of the fine-scale layering may be due to *in situ* recrystallisation (Aydin *et al.* 1994). The top of the section, northwest of Tilting, consists of coarse-grained, unfoliated plagioclase-hornblende rocks which grade to quartz dioritic agmatite containing metre-scale fragments of layered mafic rocks.

Gabbroic rocks around Seldom Come By form two ovoid masses. At Burnt Point, massive, pegmatitic gabbro contains cumulus ortho- and clinopyroxene, and large poikilitic post-cumulus amphibole and plagioclase. The body contains about 10% of sinuous, boudinaged basalt dykes up to 50 cm wide. At the head of Seldom Harbour irregularly layered gabbro and diorite grade to heterogeneous mafic rocks which contain enclaves of layered gabbro, some sharply bounded in metre-scale blocks, others apparently gradational to larger areas of massive gabbro.

The layered mafic rocks of the Fogo Island Batholith resemble large layered mafic intrusions, and imply that such a body was formed or disrupted during emplacement of the Fogo Island Batholith. Within the layered mafic rocks, abrupt reversals to a more primitive crystallisation order (clinopyroxene+plagioclase to orthopyroxene+olivine) imply repeated influx of primitive magma into a relatively stable magma chamber (Brown 1956; Wager and Brown 1968).

Gabbroic compositions commonly occur in dykes and sheets below the main batholith in the southwest corner of the island. Distinctive plagioclase-porphyrific gabbro, resembling the layered gabbro around Seldom Come By, occurs as discrete dykes, in the cores of composite dykes, as synplutonic dykes within the granite, and as synplutonic dykes within gabbro at Burnt Point.

Chemical analyses of non-cumulate gabbroic rocks from Tilting and Seldom show a considerable range of composition, ranging from subalkaline basalt across the andesite/basalt and andesite fields (Fig. 6d), a range approaching that of the apparently much more heterogeneous diorite complex (Appendix 1). On chemical discrimination diagrams (Fig. 6), compositions fall into both arc (Fig. 6a) and non-arc fields (Fig. 6b), with a large amount of scatter in some plots (Fig. 6c).

Granite

Coarse-grained granite of the Fogo Island Batholith occurs as an east-west belt across the northern part of the island, partially separated into three lobes by narrow belts of hornfelsed host rocks, agmatite, and sheets of felsite. All three lobes exhibit hastingsitic amphibole with minor biotite, and a colour index consistently <15. The central feldspar-porphyrific lobe contains 1 to 2% of digested mafic inclusions up to 5 cm across. The more equigranular eastern and western lobes lack mafic inclusions. All three lobes tend to be locally homogeneous, but become slightly more potassium feldspar-rich and leucocratic toward the north. All three lobes contain sinuous synplutonic basalt dyke segments exhibiting chilled margins, commonly 1 to 2 m wide and 5 to 10 m long (Fig. 7). Dyke lithologies

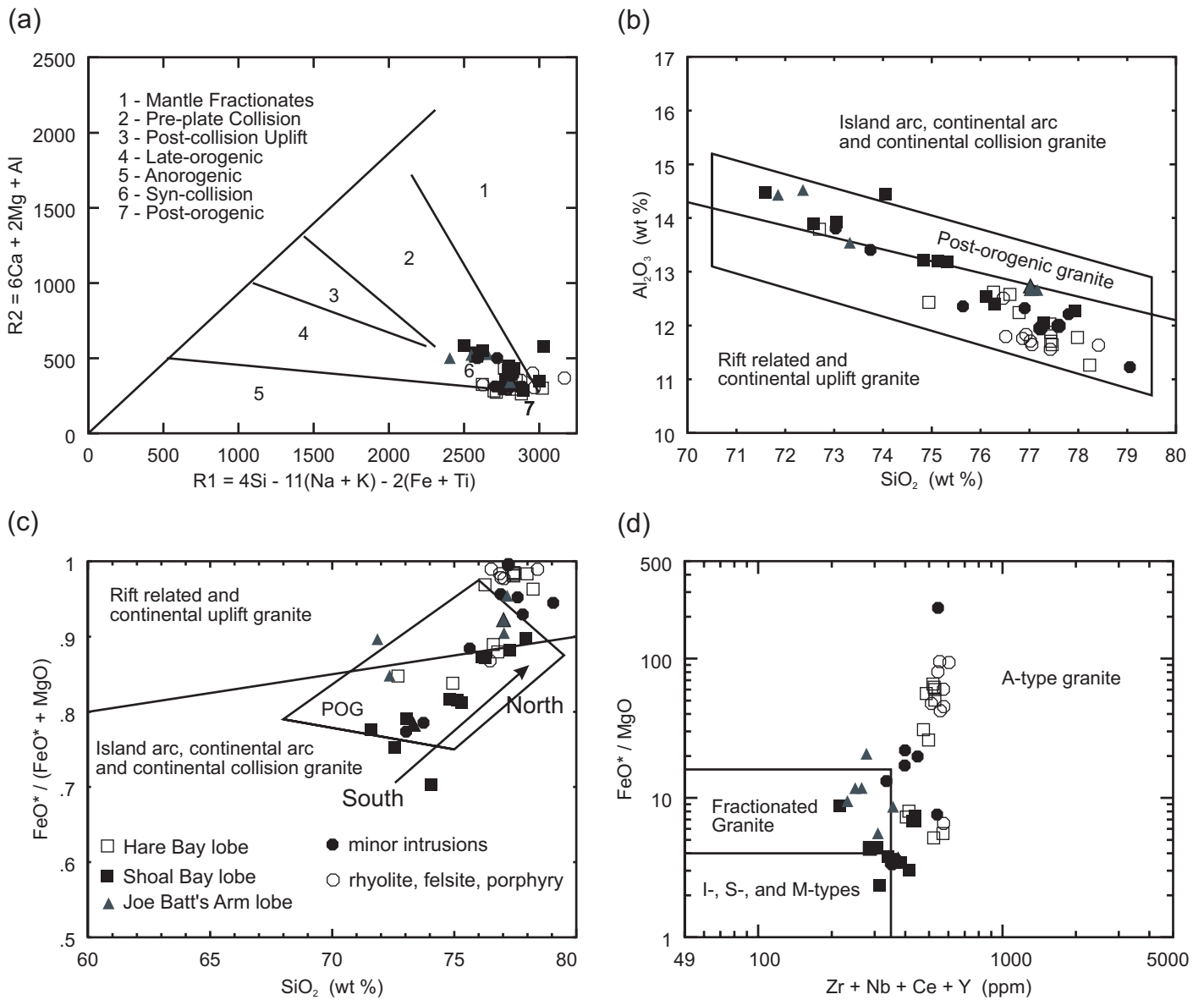


Fig. 5 Chemical data for salic rocks of the Fogo Island Batholith plotted on tectonic discrimination diagrams of (a) Batchelor and Bowden (1985), (b and c) Maniar and Piccoli (1989), and (d) Whalen *et al.* (1987).

include plagioclase-porphyratic varieties similar to the cores of composite gabbro-rhyolite dykes. Felsic dykes and pegmatite are absent and quartz veins extremely rare (one observed).

South of Fogo Harbour, granite cuts across a carapace of felsite and rhyolite sills, and is in essentially conformable contact with strongly hornfelsed sedimentary rocks. This region exhibits crude sheeting parallel to the contact, and prominent joints perpendicular to the contact.

Chemically, all analyses of the granite fall in a restricted field (Fig. 5). On the diagram of Batchelor and Bowden (1985) this region straddles the boundary between late orogenic and post-orogenic granites (Fig. 5a), whereas in the diagrams of Maniar and Piccoli (1989), it clearly falls in the post-orogenic granite field (Fig. 5b, c). The trend to more differentiated compositions from south to north in all lobes can be seen in Fig. 5c (increasing SiO_2 and $FeO^*/(FeO^*+MgO)$). The tendency toward A-type

compositions noted by Sandeman and Malpas (1995), seen in Fig. 5d, results from relatively high contents of $(Zr+Nb+Ce+Y)$ combined with extreme depletion in MgO (producing extreme FeO^*/MgO ratios). Alkali contents are not unusually high.

Diorite complex

The diorite complex forms the largest and most complex unit of the Fogo Island Batholith. Some dioritic rocks exhibit coarse, massive textures comparable to those of the gabbro and granite. However, large exposures invariably include patchy, inequigranular textures, streaks of one lithology in another, and schlieren and blocks of more mafic lithologies in a dioritic to granitic matrix. Characteristic gradational, centimetre-scale pegmatitic patches with large amphibole and feldspar crystals have widely varying alkali feldspar/plagioclase ratios, and

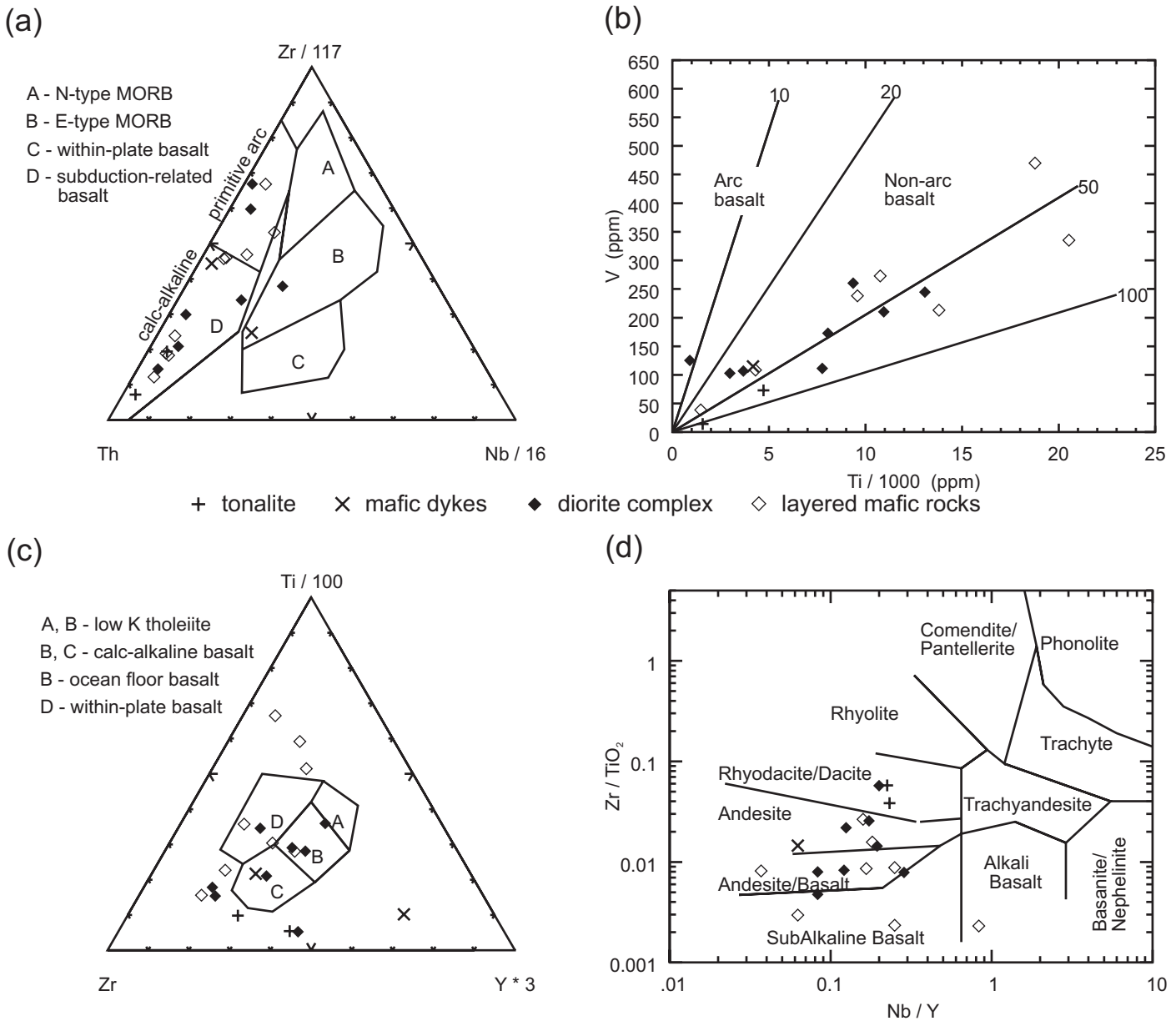


Fig. 6 Chemical data for mafic rocks of the Fogo Island Batholith plotted on tectonic discrimination diagrams of (a) Wood (1980), (b) Shervais (1982), (c) Pearce and Cann (1973), and (d) Winchester and Floyd (1977).

may contain a significant amount of quartz. Igneous breccias of diverse mafic blocks in a more silic matrix form a major part of the diorite complex (Fig. 8). The mafic component varies from rare examples of layered gabbro, to hornblende-rich amphibolite to hornblende-plagioclase rocks with minor quartz. In coastal exposures at Wild Cove, Cape Fogo, and Kippen Cove some mafic blocks exhibit intimate, amoeboid interfingering with the matrix, and form pillow-like masses, phenomena suggestive of coexisting magmas. The composition of the more homogeneous parts of the diorite complex ranges from gabbroic through hornblende diorite and quartz diorite to tonalite, monzodiorite, and rare syenite. Mafic varieties contain mafic inclusions, whereas more silic varieties contain more silicic inclusions. Much of the interior part of

the diorite complex comprises locally homogeneous, fine to medium-grained, granoblastic hornblende-plagioclase rocks with variable but minor amounts of clinopyroxene, quartz, and potash feldspar. Many of these rocks exhibit nebulous pegmatitic patches of hornblende+plagioclase, commonly associated with healed, epidote-filled fractures.

Near the contact between the diorite complex and granite, diorite and granite are typically observed in alternate outcrops, or in small adjacent areas with few exposed contact relations. In a large highway quarry, felsite and diorite form conformable, non-intrusive, metre-scale sheets. Coastal exposures at Cape Fogo and Cape Cove exhibit a variety of complex relations ranging from complexes of sills with contrasting compositions, through diorite cross-cut by granite, or pillows of mafic in silic

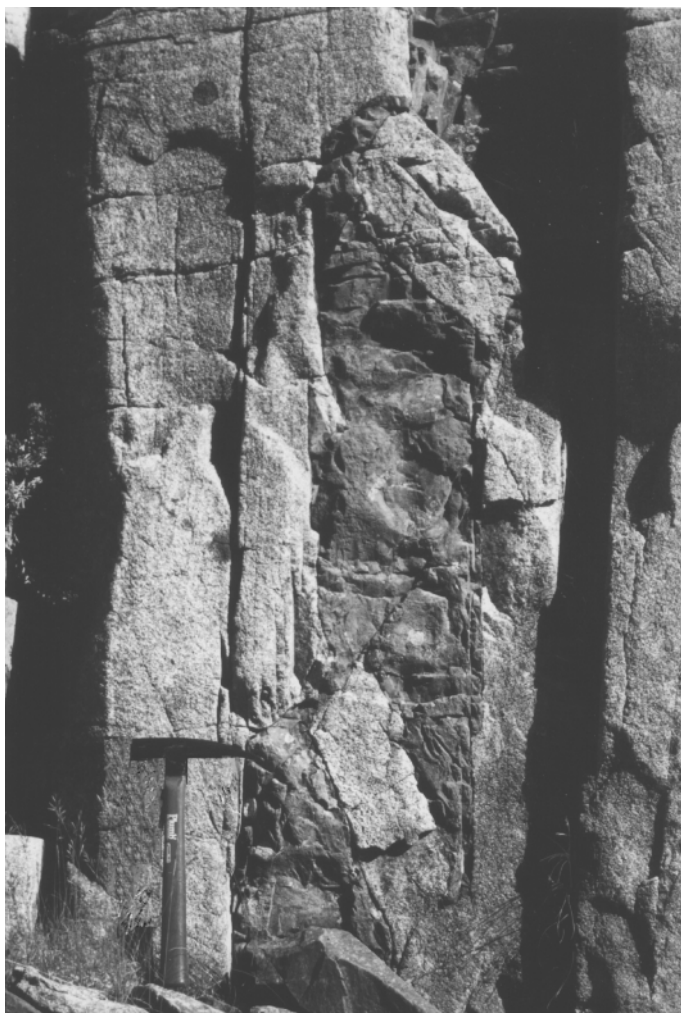


Fig. 7 Synplutonic mafic dyke segment in granite, Deep Bay. The hammer at lower left is 30 cm long.



Fig. 8 Agmatite with diorite and leucogabbro blocks in a dioritic matrix, Seldom Come By. The two elongate blocks in the lower left corner are Fogo Harbour Formation. Note the pale-coloured reaction rims on some specimens. The pen is 13 cm long.

phases, to completely gradational contacts over a few tens of centimetres. In the absence of definitive contact relations, Baird (1958) and Sandeman and Malpas (1995) interpreted the salic phases of the batholith to intrude the mafic phases. However, field observations during the present study generally suggested originally non-intrusive contacts within a zone of mingling.

Although the textural range of the diorite complex is bewilderingly large, chemical analyses (Appendix 1) show a limited range of composition, with SiO₂ content ranging fairly continuously from 52 to 61%. Two samples yielded SiO₂ contents of 64 and 75%. The former is the only one of 65 analyses of the batholith with an SiO₂ content between 61 and 70%. In general, analyses of the diorite complex plot in the same fields as the layered mafic rocks (Fig. 8) but contain much higher concentrations of K, Zr, and U, and lower contents of Mg. An obvious possible cause for these anomalies could be mixing with the granitic component of the batholith, as suggested by field observations. The strongly bimodal nature of the analyses shows that if this model is correct, mixing involved incorporation of the salic component into the mafic phase but little incorporation of the mafic component into the salic phase.

A MODEL FOR EMPLACEMENT OF THE FOGO ISLAND BATHOLITH

The Fogo Island Batholith consists of a homogeneous salic portion and a texturally heterogeneous mafic portion which includes layered rocks. A model for emplacement must explain the presence and mutual relations of these components. Field observations relevant to emplacement of the batholith may be summarised as follows. (1) Most mafic dyke emplacement and all salic dyke emplacement preceded emplacement of the main batholith and followed a near-vertical cleavage axial planar to pre-batholith open folds. (2) Composite dykes with mafic cores occur below the batholith but not above it. (3) The older part of the batholith, a thick sill, is gravitationally stratified, with mafic rocks at the base and salic rocks at the top. (4) Layered mafic rocks are disrupted by and included within heterogeneous mafic to intermediate rocks which show evidence of magma mixing and assimilation. (5) The bimodal Fogo Island Batholith developed close to a vent area of slightly older bimodal volcanic rocks of the Lawrenceton Formation.

These observations suggest a three-stage model for emplacement, namely (i) generation of a composite magma, here assumed to be due to mafic underplating of the crust with subsequent crustal anatexis, (ii) buoyant rise of the composite magma followed by gravitational differentiation to produce the sill-like mass, and (iii) a late influx of mafic magma. These stages are cartooned in Fig. 9, which uses the time scale of Tucker *et al.* (1990) for comparison of stratigraphic and absolute ages.

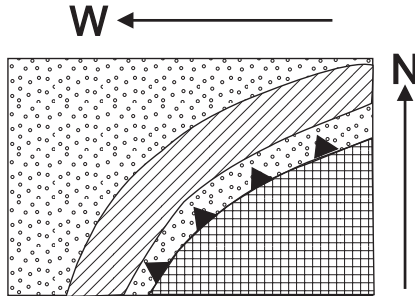
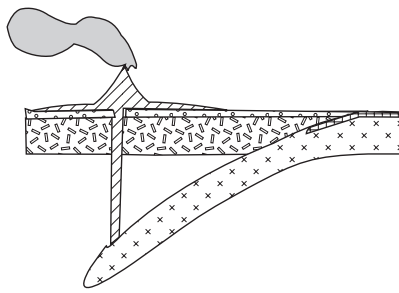
Eruption of the bimodal, subduction-related (Currie 1995) Lawrenceton Formation (Fig. 9a) had almost ceased by Late Llandovery time (~430 Ma) as motion along the Dog Bay Line

passed from subduction to dextral transpression (Karlstrom *et al.* 1982). Reduction of magmatic activity led to subsidence due to cooling of the crust, permitting a marine incursion and deposition of the Fogo Harbour Formation. Magmatism had not completely ceased, as shown by presence of tuffaceous material in the Fogo Harbour Formation. The model assumes that mafic magma, no longer able to erupt, underplated the crust where dextral transpression was converted into extension at the bend in the Dog Bay Line (Fig. 9b). The need for such a deep-seated precursor to the high-level Fogo Island Batholith follows from the regional distribution of the composite dykes which appear to have fed the batholith.

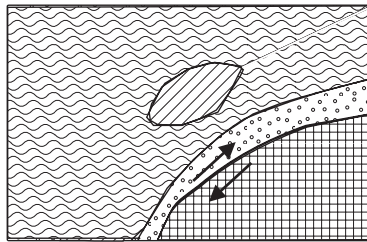
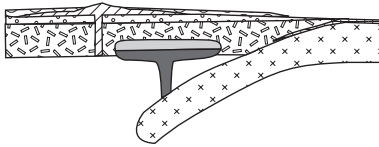
Large scale emplacement of mafic magma eventually caused anatexis of surrounding crustal host rocks, initially producing a gravitationally stable system with light salic magma above dense mafic magma. Such a system is unstable relative to its host because both components have positive buoyancy with respect to continental crust (Glazner 1994). If the volume of magma becomes sufficiently large, it will rise buoyantly along fractures. Analogs of basalt-rhyolite systems experimentally studied by Huppert and Sparks (1988) showed that fingers of hot mafic rock rise through the overlying salic melt carrying salic material along with them. The composite dykes below the Fogo Island Batholith suggest such a process, with magma following cleavage axial planar to slightly earlier folds (Fig. 9c). The large size of the dykes, and lack of mixing of salic and mafic components, suggest that these fractures may have opened during emplacement, allowing passive emplacement with the mafic magma rising to its neutral buoyancy level, and spreading laterally.

Glazner (1994) estimated the density of mafic magma near surface to be about 2.75 g/cm³, in reasonable accord with the measurement of 2.73 g/cm³ for erupting Kilauea basalt

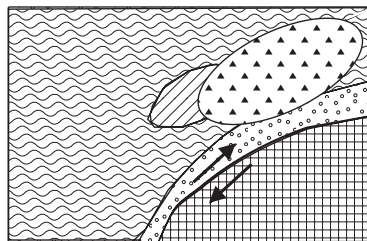
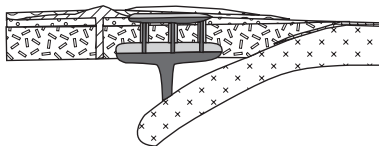
Fig. 9 (Facing page) Cartoon of a model for the emplacement of the Fogo Island Batholith. (a) ~430 Ma; Emplacement of the bimodal Lawrenceton Formation above a subduction zone. (b) ~430–422 Ma; Mafic underplating of continental crust as the effusive outlets are cut off by conversion of subduction into dextral transcurrent motion. Anatectic melt forms at the base of the crust due to the influx of heat. (c) 422 Ma; Buoyant rise of composite magma rising as dykes along axial plane cleavage to the level of neutral buoyancy. The roof is assumed to float upward, creating space. Part of the light salic fraction forms sills of felsite and porphyry, eventually reaching the surface as ignimbrites, while the mafic fraction sinks to the base. Stable conditions permit gravitational differentiation and widespread formation of igneous layering. (d) 408 Ma; A late influx of mafic magma into the body disrupts the mafic portion, producing widespread agmatization and hybridisation. The mafic magma remains below the salic rocks due to its higher density, but the high temperature and composition contrast produce double diffusive exchange across the boundary, creating local A-type granite in the salic rocks.



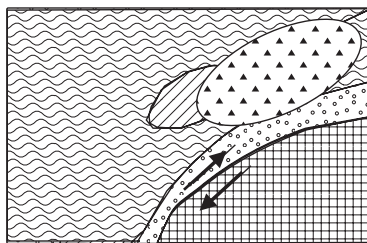
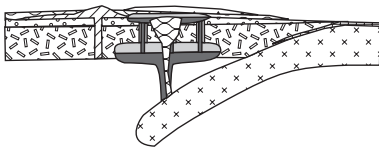
(a) ~430 Ma;
eruption of Lawrenceton
Formation



(b) ~430-422 Ma;
mafic underplating, anatexis,
surficial subsidence and
deposition due to cooling



(c) 422 Ma;
rise, spread and differentiation
of composite magma, ignimbrite
sheets erupted on floating roof



(d) 408 Ma;
emplacement of late mafic rocks,
disrupting and hybridizing with
earlier phases, formation of
"diorite"



Brimstone Head Formation;
rhyolite ignimbrite



late mafic rocks
(diorite complex)



Fogo Harbour Formation;
siltstone and tuff



granite, felsite, rhyolite



Lawrenceton Formation;
bimodal volcanic rocks



early mafic rocks,
commonly layered



Indian Islands Group;
limy siltstone, limestone



oceanic crust



mafic volcanic rocks, turbidite
(Exploits and Badger Gps.)



continental crust

(Macdonald 1963). Both values are higher than the density of Fogo Harbour Formation ($\sim 2.68 \text{ g/cm}^3$) but lower than the density of basalt of the Lawrenceton Formation ($\sim 2.89 \text{ g/cm}^3$). Currie (1995) found the latter to be underlain by a thick section of Ordovician mafic volcanic rocks and a thin section of Ordovician-Silurian greywacke (Badger Group). It is therefore plausible that mafic magma would rise buoyantly to the top of the mafic volcanic rocks, but stop near the base of the low-density Fogo Harbour Formation. The abrupt transition from submarine deposition of the Fogo Harbour Formation to the subaerial ignimbrite sheets of the Brimstone Head Formation required rapid uplift which could be explained by floating of the Fogo Harbour Formation on underlying magma, combined with thermal expansion.

The thick composite dykes intruding the Fogo Harbour Formation strongly suggest that the magma was composite when emplaced. Gravitational differentiation of such composite magma would lead to formation of salic upper and mafic lower parts. Because the density of the salic portion would be less than that of the host Fogo Harbour Formation, it could continue to rise, hypothetically producing the three observed domes and their dividing screens of agmatite. Given sufficient heat content and appropriate channels, it could eventually reach the surface and erupt to form ignimbrite sheets (Brimstone Head Formation).

The proposed model requires passive conditions of emplacement. Layered mafic rocks, the presence of composite dykes, and apparent large-scale gravitational differentiation of composite magma all indicate stable conditions. Repetition of cumulus assemblages (olivine + orthopyroxene) in the layered gabbro suggests that minor influxes of fresh mafic magma did not disturb these conditions. However, influx of a large volume of mafic magma (Fig. 9d) would upset the delicate thermal steady state producing vigorous convection and hybridisation with slightly older, still hot, phases of the batholith. Along contacts with salic rocks, remelting could form some salic liquid, leading to the formation of complex salic-mafic relations, including pillow-like masses of mafic rocks in salic matrices, and some cross-cutting of mafic rocks by salic dykes. Conditions along such interfaces would favour extensive double diffusive transfer of material across the boundary, leading to A-type tendencies in the overlying granite according to the model of Wiebe (1994).

The present superb exposure of internal structure of the Fogo Island Batholith results from tipping of the batholith at a moderate angle to the northwest subsequent to emplacement by minor late sinistral movement on the Dog Bay Line (Williams *et al.* 1993; Piasecki 1992) which produced compression in the Fogo Island region in early to mid-Devonian time.

ACKNOWLEDGEMENTS

This is Geological Survey of Canada Contribution Number 1997066. The author wishes to acknowledge constructive reviews of a previous version of the paper by Louise Corriveau

and two anonymous referees, and a concise and helpful review by an anonymous journal reviewer.

REFERENCES

- AYDIN, N.S. 1995. Petrology of the composite mafic-felsic rocks of the Fogo Island batholith: A window to mafic magma chamber processes and the role of mantle in the petrogenesis of granitoid rocks. Ph.D. thesis, Memorial University of Newfoundland, St. John's, Newfoundland. 191 p.
- AYDIN, N.S., MALPAS, J., & JENNER, G. 1994. Physical characteristics of the Tilting Layered Suite, Fogo Island, Newfoundland. *African Journal of Geology*, 97, pp. 496–506
- BAIRD, D.M. 1958. *Fogo Island map-area, Newfoundland*. Geological Survey of Canada. Memoir 301, 63 p.
- BATCHELOR, R.A., & BOWDEN, P. 1985. Petrogenetic interpretation of granitoid rock series using multicationic parameters. *Chemical Geology*, 48, pp. 43–55.
- BROWN, G.M. 1956. The layered ultramafic rocks of Rhum, Inner Hebrides. *Philosophical Transactions of the Royal Society*, A240, pp. 1–53.
- CAWTHORN, R.G. 1978. The petrology of the Tilting Harbour igneous complex, Fogo Island, Newfoundland. *Canadian Journal of Earth Sciences*, 16, pp. 526–539.
- CURRIE, K.L. 1995. The northeast end of the Dunnage Zone in Newfoundland. *Atlantic Geology*, 31, pp. 25–38.
- CURRIE, K.L. 1997a. A note on the geology of Change Islands, Newfoundland. Geological Survey of Canada Current Research, 1997-D, pp. 51–55.
- CURRIE, K.L. 1997b. Geology of Fogo Island, Newfoundland - a study of form and emplacement of igneous intrusions. Geological Survey of Canada Current Research, 1997-D, pp. 45–54.
- CURRIE, K.L. 1997c. Fogo map-area, Newfoundland. Geological Survey of Canada Open File 3466.
- CURRIE, K.L., & PAJARI, G.E. 1981. Anatectic peraluminous granites from the Carmanville area, northeastern Newfoundland. *Canadian Mineralogist*, 19, pp. 147–161.
- D'LEMONS, R.S., & HOLDSWORTH, R.E. 1995. Samarium-neodymium isotope characteristics in the northeast Gander Zone. Geological Association of Canada Special Paper, 41, pp. 239–252.
- ELLIOT, C.G., DUNNING, G.R., & WILLIAMS, P.F. 1991. New U/Pb zircon age constraints on the timing of deformation in north central Newfoundland and implications for early Paleozoic Appalachian orogenesis. *Geological Society of America Bulletin*, 103, pp. 125–135.
- GLAZNER, A.F. 1994. Foundering of mafic plutons and density stratification of continental crust. *Geology*, 22, pp. 435–438.
- HUPPERT, H.E., & SPARKS, R.S.J. 1988. The fluid dynamics of crustal melting by injection of basaltic sills. *Transactions of the Royal Society of Edinburgh, Earth Sciences*, 79, pp. 237–243.
- KARLSTROM, K.E., VAN DER PLUIJM, B.A., & WILLIAMS, P.F. 1982. Structural interpretation of the eastern Notre Dame

- Bay area, Newfoundland. Regional post-Middle Silurian thrusting and asymmetrical folding. *Canadian Journal of Earth Sciences*, 19, pp. 2325–2341.
- KERR, A., HAYES, J.P., COLMAN-SADD, S.P., DICKSON, W.L., & BUTLER, J. 1993. An integrated lithochemical data base for the granitoid plutonic suites of Newfoundland. Unpublished contract report under the Canada-Newfoundland Mineral Development Agreement, 433 p.
- MACDONALD, G.A. 1963. Physical properties of erupting Hawaiian magmas. *Bulletin of the Geological Society of America*, 74, pp. 1071–1078.
- MANIAR, P.D., & PICCOLI, P.M. 1989. Tectonic discrimination of granitoids. *Geological Society of America Bulletin*, 101, pp. 635–643.
- O'BRIEN, B.H., SWINDEN, H.S., DUNNING, G.R., WILLIAMS, S.H., & O'BRIEN, F.H.C. 1997. A peri-Gondwanan arc-back arc complex in Iapetus: early mid-Ordovician evolution of the Exploits Group, Newfoundland. *American Journal of Science*, 297, pp. 220–272.
- PATERSON, S.R., & VERNON, R.H. 1995. Bursting the bubble of ballooning plutons: a return to nested diapirs emplaced by multiple processes. *Geological Society of America Bulletin*, 107, pp. 1356–1380.
- PEARCE, J.A., & CANN, J.R. 1973. Tectonic setting of basic volcanic rocks determined using trace element analyses. *Earth and Planetary Science Letters*, 19, pp. 290–300.
- PETFORD, N. 1996. Dykes and diapirs? *Transactions of the Royal Society of Edinburgh, Earth Sciences*, 87, pp. 105–114.
- PIASECKI, M.A.J. 1992. Tectonics across the Gander-Dunnage boundary in northeastern Newfoundland. *Geological Survey of Canada Paper*, 92-1E, pp. 259–268.
- SANDEMAN, H.A., & MALPAS, J. 1995. Epizonal I and A-type granites and associated ash-flow tuffs, Fogo Island, northeast Newfoundland. *Canadian Journal of Earth Sciences*, 32, pp. 1832–1844.
- SHERVAIS, J.W. 1982. Ti-V plots and the petrogenesis of modern and ophiolitic lavas. *Earth and Planetary Science Letters*, 59, pp. 101–118.
- SYLVESTER, A.G. 1964. The Precambrian rocks of the Telemark area in south-central Norway. III. Geology of the Vrådal granite. *Norsk Geologiske Tidsskrifter*, 44, pp. 445–482.
- TUCKER, R.D., KROGH, T.E., ROSS, R.J., & WILLIAMS, S.H. 1990. Time-scale calibration by high-precision U-Pb zircon dating of interstratified volcanic ashes in the Ordovician and Lower Silurian stratotypes of Britain. *Earth and Planetary Science Letters*, 100, pp. 51–58.
- WAGER, L.R., & BROWN, G.M. 1968. *Layered Igneous Rocks*. Oliver and Boyd, London. 588 p.
- WEINBERG, R.F. 1996. Ascent mechanisms of felsic magmas. *Transactions of the Royal Society of Edinburgh, Earth Sciences*, 87, pp. 95–103.
- WHALEN, J.B., CURRIE, K.L., & CHAPPELL, B. W. 1987. A-type granites: geochemical characteristics, discrimination and petrogenesis. *Contributions to Mineralogy and Petrology*, 95, pp. 407–419.
- WIEBE, R.A. 1994. Silicic magma chambers as traps for basaltic magmas: the Cadillac Mountain intrusive complex, Mount Desert Island, Maine. *Journal of Geology*, 102, pp. 423–437.
- WILLIAMS, H. 1972. Stratigraphy of Botwood map-area, north-eastern Newfoundland. *Geological Survey of Canada Open File*, 113, 98 p.
- WILLIAMS, H., CURRIE, K.L., & PIASECKI, M.A.J. 1993. The Dog Bay Line, a Silurian terrane boundary in northeast Newfoundland. *Canadian Journal of Earth Sciences*, 29, pp. 2481–2494.
- WILLIAMS, H., DEAN, P.L., & PICKERING, K.T. 1995. Botwood Belt. *In* *Geology of the Appalachian-Caledonide Orogen in Canada*. Edited by H. Williams. *Geological Survey of Canada, Geology of Canada*, 6, pp. 413–420.
- WINCHESTER, J.A., & FLOYD, P.A. 1977. Geochemical discrimination of different magma series and their differentiation products using immobile elements. *Chemical Geology*, 20, pp. 325–343.
- WOOD, D.A. 1980. The application of a Th-Hf-Ta diagram to problems of tectonomagmatic classification and to establishing the nature of crustal contamination of basaltic lavas of the British Tertiary volcanic province. *Earth and Planetary Science Letters*, 50, pp. 11–30.

Editorial responsibility: Sandra M. Barr

Appendix 1. Geochemical data for the Fogo Island Batholith.

Unit Sample #	Hare Bay lobe					Shoal Bay lobe												
	K05	K06	K07	K10	K19	K21	K31	K34	K42	K03	K09	K16	K18	K26	K27	K40	K44	K46
SiO ₂	77.35	77.25	77.15	76.70	76.05	75.95	75.40	74.25	71.80	77.54	76.80	76.40	76.15	75.90	75.75	72.95	71.50	70.60
TiO ₂	0.17	0.11	0.12	0.11	0.18	0.13	0.17	0.35	0.36	0.09	0.12	0.20	0.19	0.20	0.21	0.32	0.40	0.38
Al ₂ O ₃	11.14	11.68	11.65	11.53	12.49	11.80	12.48	12.32	13.62	12.21	11.78	11.91	12.14	12.34	12.48	13.91	13.68	14.28
Fe ₂ O ₃	0.43	0.98	1.22	0.69	0.46	0.50	1.15	0.29	0.44	0.42	0.98	0.48	2.03	0.39	0.06	0.48	0.59	0.65
FeO	1.96	1.09	0.70	1.25	1.52	1.24	0.82	2.69	2.77	0.85	1.14	1.58	<1.0	1.68	2.08	2.07	2.30	2.25
MnO	0.05	0.03	0.03	0.03	0.03	0.03	0.03	0.06	0.07	0.02	0.03	0.03	0.03	0.03	0.04	0.05	0.06	0.05
MgO	0.09	0.03	0.03	0.03	0.24	0.03	0.06	0.57	0.14	0.14	0.04	0.27	0.25	0.30	0.31	0.66	0.93	0.82
CaO	0.70	0.40	0.28	0.49	0.59	0.59	0.70	1.48	2.15	0.38	0.55	0.90	0.94	0.93	0.93	1.99	2.12	2.39
Na ₂ O	3.85	3.84	3.52	3.88	3.43	3.83	4.09	3.87	4.25	3.44	3.75	3.40	3.78	3.54	3.54	3.96	3.94	3.97
K ₂ O	3.11	4.34	4.21	4.29	4.26	3.97	3.94	3.15	2.66	4.39	3.98	3.65	3.63	4.17	4.10	3.41	2.94	3.15
P ₂ O ₅	0.02	0.01	0.02	0.01	0.03	0.03	0.02	0.05	0.07	0.01	0.01	0.03	0.03	0.02	0.02	0.06	0.06	0.07
LOI	0.65	0.58	0.50	0.63	0.65	0.47	0.59	0.76	0.46	0.35	0.83	0.39	0.67	0.52	0.54	0.56	0.75	0.74
Total	99.52	100.34	99.43	99.64	99.93	98.57	99.45	99.84	99.22	99.84	100.01	99.24	99.84	100.02	100.06	100.42	99.27	99.35
Trace element contents in ppm																		
Li	9.2	10.3	3.2	13	12.3	14.8	4	28.7	26.4	11.9	5.8	43.3	22.9	36.2	37.8	36.4	41.3	33.7
Be	3.4	3.8	4.1	4.3	2.9	4.3	3.7	2.5	3.3	2.7	3.1	3.3	3.6	3.6	3.6	3.8	2.3	2.5
F	131	541	99	669	451	399	101	404	380	64	656	386	339	630	523	555	551	133
V	1	1	1	1	8	4	5	22	28	2	1	9	10	9	9	26	34	34
Cr	2	2	1	1	3	2	3	7	9	2	1	5	3	5	5	8	11	10
Co	1	1	1	2	2	2	3	5	6	1	3	2	2	2	2	5	5	6
Ni	3	1	2	3	1	1	1	5	4	3	2	1	3	6	2	5	6	4
Cu	9	7	7	12	5	8	9	4	10	8	6	7	5	11	7	6	4	4
Zn	56	54	42	67	26	63	41	60	72	25	43	42	42	42	43	41	53	46
Ga	20	22	20	21	22	22	22	19	22	20	20	22	20	19	23	23	19	23
Rb	115	150	150	140	140	141	82	95	80	175	115	145	125	160	155	140	105	110
Sr	109	43	43	42	69	45	92	134	146	24	70	55	67	58	56	99	160	128
Y	71	93	93	98	63	77	62	65	50	40	97	66	80	83	84	57	58	56
Zr	330	270	269	271	174	266	301	327	420	132	258	247	199	219	219	186	261	228
Nb	16	22	19	17	12	19	20	15	16	9	18	14	15	14	13	14	11	11
Mo	5	4	4	4	3	3	3	7	4	4	4	4	4	4	5	4	4	4
Ba	659	612	543	555	565	561	620	793	657	102	700	475	477	463	456	347	678	397
La	35	61	67	62	74	55	27	52	36	24	66	47	50	58	61	34	38	35
Ce	76	134	143	134	162	117	87	111	78	34	152	106	107	112	122	83	80	82
Pb	1	5	5	13	1	12	9	3	9	11	1	1	3	8	5	3	1	3
Th	9	17	18	16	20	17	13	13	11	30	17	17	16	18	18	18	4	13
U	3	4.6	5	4.5	3.6	5.4	3.3	2.7	2.9	9	4.5	4.1	5.1	5.3	6.1	4	1.8	3.4

Data from Kerr *et al.* (1993). Samples were collected by A. Kerr in 1990 and 1991, and analysed by H. Wagenbauer, Newfoundland Geological Surveys Branch. Major element analyses were by ICP-ES except for LOI (gravimetric) and FeO (titration). Trace element analyses were by ICP-ES with F by ISE. Accuracy and precision were extensively discussed by J.P. Hayes in Kerr *et al.* (1993).

Appendix 1. (cont'd.)

Unit Sample #	Joe Batts Arm lobe										Minor felsic bodies									
	K11	K12	K20	K29	K35	K36	K37	K41	K47	K04	K14	K15	K22	K24	K25	K28	K38	K43		
SiO ₂	76.65	76.65	76.05	75.50	74.05	74.00	73.90	72.55	70.05	77.45	76.45	76.40	75.95	75.95	75.95	75.75	73.25	71.50		
TiO ₂	0.16	0.15	0.13	0.15	0.28	0.28	0.27	0.30	0.30	0.16	0.17	0.16	0.17	0.18	0.16	0.19	0.34	0.30		
Al ₂ O ₃	12.62	12.67	12.48	12.41	13.09	12.96	12.99	14.15	14.07	11.49	11.76	11.78	11.55	11.62	11.48	11.31	13.53	14.35		
Fe ₂ O ₃	0.65	0.61	0.63	0.48	0.52	0.49	0.52	0.59	0.80	0.59	0.78	1.43	0.99	2.68	0.45	1.22	0.25	0.88		
FeO	0.84	0.87	0.68	0.98	1.85	1.59	1.74	0.94	2.49	1.35	1.56	1.57	1.52	<10	2.14	1.77	2.44	2.22		
MnO	0.03	0.04	0.03	0.03	0.06	0.05	0.05	0.08	0.09	0.04	0.10	0.04	0.04	0.05	0.03	0.04	0.05	0.08		
MgO	0.15	0.12	0.06	0.12	0.52	0.47	0.50	0.62	0.37	0.02	0.05	0.03	0.03	0.04	0.06	0.06	0.74	0.54		
CaO	0.62	0.61	0.66	0.81	1.52	1.25	1.38	2.43	1.82	1.29	1.55	0.71	0.72	1.12	0.77	0.68	2.10	1.95		
Na ₂ O	3.70	3.93	3.96	3.88	3.71	3.71	3.59	2.94	4.01	4.00	3.80	3.92	3.98	3.85	3.84	3.86	3.89	4.42		
K ₂ O	4.05	3.86	3.82	3.66	3.31	3.41	3.39	3.29	3.42	2.36	3.15	3.80	3.65	3.31	3.68	2.94	3.25	2.49		
P ₂ O ₅	0.02	0.01	0.05	0.01	0.05	0.05	0.04	0.09	0.07	0.02	0.01	0.01	0.01	0.01	0.01	0.01	0.06	0.08		
LOI	0.69	0.59	0.66	0.47	0.78	0.83	0.81	1.42	0.69	0.20	0.98	0.31	0.56	1.05	0.69	0.39	0.49	0.80		
Total	100.18	100.11	99.21	98.50	99.74	99.09	99.18	99.40	98.18	98.97	100.36	100.16	99.17	99.86	99.26	98.22	100.39	99.61		
Trace element contents in ppm																				
Li	14.6	11.3	7.5	20.2	26.8	25.2	18.8	15.1	46.5	2.4	6.4	0.6	1.8	4.4	2.2	2.8	33.5	13.6		
Be	1.9	1.9	2.7	1.7	2.4	2.3	2.6	2.1	2.1	3.4	2.8	3.3	3.3	3.2	3.7	2.7	2.8	1.9		
F	127	499	267	323	301	473	376	298	318	78	101	65	132	108	81	95	511	260		
V	4	2	4	2	19	17	18	16	13	1	1	1	1	1	1	1	30	12		
Cr	2	1	1	3	5	5	5	6	3	1	3	2	1	7	4	1	9	6		
Co	1	1	2	3	4	4	4	3	3	1	2	1	1	1	1	1	5	5		
Ni	1	1	1	1	5	3	8	5	1	1	2	6	1	2	1	1	8	2		
Cu	8	9	10	4	27	10	6	8	5	11	14	12	10	17	20	8	8	15		
Zn	36	51	41	38	75	51	37	87	63	26	204	45	47	44	106	28	54	67		
Ga	16	16	17	14	19	21	21	15	22	21	21	21	21	21	21	21	20	21		
Rb	135	135	128	115	120	130	125	115	110	25	70	115	100	70	110	65	110	75		
Sr	66	58	64	58	136	107	115	138	132	216	141	67	82	106	65	107	109	150		
Y	26	36	36	32	42	40	46	42	34	91	79	86	88	78	80	66	71	37		
Zr	149	160	164	142	156	168	174	192	222	353	356	322	302	355	328	322	208	204		
Nb	6	9	10	6	10	9	10	9	11	20	19	19	18	17	20	16	12	9		
Mo	5	4	3	4	5	4	4	3	5	3	4	5	3	4	4	4	4	3		
Ba	419	394	403	381	405	438	499	535	431	776	914	629	686	744	618	672	483	285		
La	23	27	30	30	36	31	33	32	36	55	48	52	53	45	48	43	32	26		
Ce	50	59	64	65	74	65	71	65	81	133	118	125	129	117	121	97	83	56		
Pb	10	9	17	1	18	11	9	40	2	1	26	1	1	1	1	1	4	1		
Th	12	13	15	8	14	13	16	14	9	14	13	14	12	13	14	10	10	9		
U	4.1	3.2	5.7	3.5	3.1	3.2	4.3	3.5	3.1	4.4	4.1	4.6	4	4	4.3	2.8	2.6	2.3		

Appendix 1. (cont'd.)

Unit Sample #	Rhyolite, felsite, porphyry								Gabbro								
	K01	K02	K08	K13	K17	K32	K33	K39	K45	K57	K58	K59	K60	K62	K63	K64	K66
SiO ₂	77.95	77.85	77.00	76.45	76.25	75.25	75.10	73.20	71.20	53.55	53.05	52.65	51.00	50.50	49.45	49.25	45.15
TiO ₂	0.15	0.11	0.16	0.15	0.16	0.26	0.28	0.34	0.34	0.49	1.56	0.61	1.80	1.79	5.03	3.36	0.24
Al ₂ O ₃	11.07	12.22	11.90	11.83	12.22	12.31	12.27	13.31	13.46	4.40	16.33	18.04	18.85	17.09	18.17	7.96	13.37
Fe ₂ O ₃	0.52	0.16	0.52	1.52	0.71	0.54	0.57	0.08	0.29	1.61	0.05	1.54	3.67	2.96	2.75	3.47	2.94
FeO	1.59	0.78	1.32	0.95	1.12	1.09	2.23	2.56	2.40	5.14	8.79	4.07	4.87	6.35	6.29	12.21	8.24
MnO	0.03	0.03	0.04	0.06	0.03	0.01	0.05	0.06	0.05	0.14	0.21	0.12	0.13	0.15	0.13	0.26	0.18
MgO	0.12	0.07	0.09	0.01	0.08	0.24	0.36	0.72	0.78	18.88	6.23	7.33	4.35	6.49	4.32	12.70	19.40
CaO	0.60	0.62	0.66	0.81	0.62	0.61	1.22	1.88	1.74	12.80	9.40	11.89	7.89	10.60	9.05	6.72	6.42
Na ₂ O	3.23	3.03	3.68	4.63	4.01	4.06	3.66	3.66	3.79	0.92	3.14	2.71	4.17	3.23	3.79	1.48	1.55
K ₂ O	3.33	5.18	3.85	2.56	3.93	4.00	3.50	3.39	3.38	0.44	0.88	0.30	1.38	0.39	0.50	0.51	0.20
P ₂ O ₅	0.01	0.01	0.01	0.03	0.02	0.04	0.05	0.06	0.06	0.05	0.20	0.14	0.42	0.14	0.11	0.16	0.06
LOI	0.33	0.34	0.38	0.39	0.33	0.60	0.51	0.86	0.86	1.50	0.98	0.67	2.02	0.91	0.63	1.92	2.90
Total	98.93	100.40	99.61	99.39	99.48	99.01	99.80	100.12	98.35	99.92	100.82	100.07	100.55	100.60	100.22	100.00	100.65
Trace element contents in ppm																	
Li	8.9	3.8	6.7	1.8	6.7	4.1	13.3	26.5	31.3	11.4	16.8	6	13.5	7.2	9.8	8.2	5.3
Be	2.2	1.9	3.3	4.1	3.5	3.3	2.2	2.9	2.8	0.4	1.2	1.7	1.2	0.7	1.5	1	0.3
B	122	37	489	85	161	293	213	494	469	241	279	132	417	120	56	167	97
V	5	5	2	1	3	9	15	30	32	101	260	106	207	272	293	329	38
Cr	2	2	2	1	2	2	6	9	9	1270	167	167	82	196	97	487	406
Co	1	1	1	1	1	1	3	6	5	69	26	30	29	40	35	77	97
Ni	2	1	1	1	1	11	2	7	7	522	1	35	50	41	76	206	298
Cu	12	4	4	29	13	13	16	15	8	94	14	28	34	37	61	109	12
Zn	55	21	57	67	58	16	64	53	49	58	91	51	76	70	54	115	89
Ga	20	21	21	22	20	18	22	20	19	12	24	22	24	22	25	23	15
Rb	85	150	115	52	125	105	75	110	120	10	20	10	35	5	10	10	10
Sr	49	73	49	88	48	156	92	142	143	114	239	689	897	654	594	212	365
Y	69	35	78	78	52	65	75	59	65	12	33	12	21	16	12	20	4
Zr	202	201	234	325	232	366	331	214	180	39	129	29	141	53	116	79	21
Nb	12	6	18	20	20	18	16	11	11	1	4	1	6	1	10	5	1
Mo	3	4	4	3	4	5	4	4	3	4	6	4	5	4	5	4	4
Ba	499	948	572	753	588	828	785	534	472	84	127	126	508	159	132	74	82
La	48	45	50	50	33	46	50	38	40	8	15	11	37	10	9	10	6
Ce	110	93	116	117	92	116	114	79	88	24	35	25	75	23	16	27	12
Pb	6	8	11	8	6	1	7	5	8	5	1	2	3	1	1	8	1
Th	14	9	16	14	16	12	8	13	17	1	1	1	5	1	1	1	1
U	2.8	1.8	4	3.8	2.6	3.7	1.7	3.5	3.7	0.5	1.5	0.3	1.1	0.4	0.6	0.7	0.3

Appendix 1. (cont'd.)

Unit Sample #	Tonalite, grandt.				Diorite complex				Mafic dykes					
	K30	K48	K49	K50	K51	K52	K53	K54	K55	K56	K61	K65		
SiO ₂	75.40	64.25	59.45	59.35	58.60	57.75	57.65	55.45	54.60	54.20	50.60	48.45		
TiO ₂	0.26	0.78	0.68	0.71	0.15	1.33	2.14	2.25	1.28	1.58	3.08	0.42		
Al ₂ O ₃	12.87	15.54	17.17	15.99	18.58	17.66	13.17	13.07	16.18	16.48	14.66	4.30		
Fe ₂ O ₃	0.37	3.40	0.87	1.29	1.75	0.27	1.83	1.51	1.47	0.93	2.55	6.96		
FeO	1.89	3.06	4.79	4.11	0.37	6.51	9.43	10.55	9.44	7.82	10.19	12.88		
MnO	0.07	0.06	0.10	0.10	0.21	0.15	0.22	0.24	0.24	0.23	0.22	0.08		
MgO	0.54	0.61	3.23	5.57	0.24	2.80	2.44	2.48	3.91	5.09	4.10	12.78		
CaO	2.13	3.91	6.54	6.42	15.17	7.02	5.66	6.45	7.10	7.82	8.37	11.22		
Na ₂ O	4.26	3.93	3.31	3.39	1.71	3.72	3.35	3.22	3.24	3.00	3.20	0.77		
K ₂ O	1.44	3.29	1.29	1.61	2.26	1.52	1.40	1.46	1.01	1.44	0.70	0.44		
P ₂ O ₅	0.05	0.19	0.13	0.17	0.02	0.20	0.81	1.00	0.29	0.19	0.66	0.05		
LOI	1.11	0.82	1.93	1.56	1.40	1.37	2.26	1.42	1.22	1.72	0.20	2.01		
Total	100.39	99.84	99.49	100.27	100.46	100.30	100.36	99.10	99.98	100.50	98.53	100.36		
Trace element contents in ppm														
Li	21.9	33.2	56.1	18.3	2.2	36.5	23.7	29.7	13	41.6	14.2	14		
Be	1.7	2.1	0.9	1.2	9.7	1.8	2.1	1.7	1.3	1.5	2	1.7		
F	294	334	190	291	391	350	683	750	271	412	429	3369		
V	14	72	112	107	124	171	240	208	110	235	462	72		
Cr	26	11	43	217	4	76	3	2	87	201	26	11		
Co	6	8	21	26	1	13	23	19	25	19	3	55		
Ni	15	6	20	128	4	10	8	1	22	2	21	33		
Cu	60	115	3	28	11	21	27	27	13	15	24	9		
Zn	146	52	60	66	234	88	116	106	99	102	101	148		
Ga	19	23	22	21	43	26	27	28	29	25	36	25		
Rb	55	65	75	20	55	45	45	50	25	45	18	5		
Sr	132	247	258	484	573	275	296	272	366	218	317	22		
Y	40	43	16	11	25	36	52	44	24	36	27	56		
Zr	150	300	99	112	86	191	548	597	280	135	251	55		
Nb	9	10	1	2	5	7	9	7	3	6	1	7		
Mo	4	5	4	4	5	5	5	5	5	5	4	5		
Ba	264	535	121	286	753	245	514	249	330	414	123	27		
La	34	35	10	18	20	25	27	23	13	19	14	55		
Ce	71	80	23	38	36	51	77	54	30	44	39	131		
Pb	50	11	1	1	274	1	5	9	1	1	1	11		
Th	16	10	1	1	5	1	5	3	1	4	1	1		
U	4	4.5	1.2	1.2	2.3	3	2.1	1.4	1	2.4	0.8	0.6		

Appendix 2. Sample locations.

#	Eastings	Northing	Description	#	Eastings	Northing	Description
Hare Bay lobe							
K05	693360	5504100	granite, shore south of Hare Bay Head	K38	715560	5505400	granite, 2 km northwest of Cape Fogo
K06	695200	5503000	granite, Leveret Islands	K43	712900	5508730	granite, Olivers Cove
K07	693700	5505800	granite, Hare Bay Head	Felsite, porphyry and microgranite			
K10	694850	5506400	granite, Leveret Islands	K01	693570	5597700	felsite, coast south of Island Harbour
K19	695930	5504600	granite, road cut at Deep Bay	K02	713890	5503840	felsite, Cape Cove
K21	696000	5504200	granite, Island Harbour-Deep Bay junction	K08	701310	5501780	porphyry, Highway 333 at Mile Pond
K31	694750	5503000	granite, road to Island Harbour	K13	702050	5500880	microgranite, highway 2 km northwest of Seldom
K34	697280	5504200	granite, head of Hare Bay	K17	700200	5497750	rhyolite dyke, highway at Little Seldom Cove
K42	699050	5503950	granite, road to Island Harbour 2 km west of highway	K32	716000	5503600	felsite, coast 1 km west of Cape Fogo
Shoal Bay lobe							
K03	700520	5509460	granite, west side of Shoal Bay	K33	712140	5501750	porphyritic rhyolite, West Head
K09	695100	5508100	granite, head northeast of Hare Bay	K39	714090	5504650	microgranite, central part of Cape Fogo peninsula
K16	700520	5509460	granite, west side of Shoal Bay	K45	713160	5503800	felsite, Cape Cove
K18	696650	5505470	granite, east side of Hare Bay	Diorite complex, tonalite			
K26	697910	5507660	granite, 4 km southeast of Fogo	K30	708540	5514100	tonalite, Round Head
K27	699640	5505300	granite, Highway 333 1 km north of Highway 334	K48	712140	5501750	heterogeneous granodiorite, Western Head
K40	702350	5509580	grained granite, Highway 334 2 km north of Shoal Bay	K49	701280	5506840	diorite dyke in granite, south tip of Shoal Bay
K44	701280	5505840	grained granite, Highway 334 2 km southwest of Shoal Bay	K50	712220	5510000	diorite, east side of Tilting Harbour
K46	702400	5506500	grained granite, Highway 334 1 km south of Shoal Bay	K51	708540	5514100	diorite agmatite, Round Head
Joe Batts Arm lobe							
K11	706580	5510800	granite, Highway 333 4 km east of Joe Batts Arm	K52	700350	5503100	diorite, highway quarry near Island Harbour turnoff
K12	705450	5511530	granite, Highway 334, Joe Batts Arm	K53	697910	5495500	diorite, dyke or minor intrusion, Cobb Cove
K20	707250	5511100	granite, Highway 333 5 km east of Joe Batts Arm	K54	701650	5497760	diorite, highway at Little Seldom
K29	709130	5510530	granite, Highway 333 7 km east of Joe Batts Arm	Massive and layered gabbro			
K35	708160	5514290	granite, shore west of Round Head	K55	704360	5498700	gabbro, east side of Seldom Harbour
K36	704420	5513850	granite, shore north of Joe Batts Arm	K56	713160	5503800	gabbro inclusion in diorite, Cape Cove
K37	705320	5514420	granite, head 3 km north of Joe Batts Arm	K57	713000	5509600	gabbro, head shore of Tilting Harbour
K41	708840	5514100	granite, Round Head	K58	714060	5503330	heterogeneous gabbro, Cape Cove
K47	708040	5510600	granite, Highway 333 6- km east of Joe Batts Arm	K59	710450	5510000	layered gabbro, Sandy Cove
Minor felsic intrusions							
K04	697460	5494290	granite, west side of Stag Harbour	K60	710820	5510310	gabbro, Sandy Cove
K14	697180	5494300	granite, west side of Stag Harbour	K62	710700	5510060	gabbro, Sandy Cove
K15	700150	5497450	granite, highway northwest corner of Little Seldom Cove	K63	711800	5510150	gabbro, northwest corner of Tilting Harbour
K22	697910	5495500	granite, Cobb Cove	K64	711800	5510150	gabbro, northwest corner of Tilting Harbour
K24	695110	5494350	granite sill, ferry landing at Man o' War Cove	K66	711000	5510360	gabbro, shore between Tilting and Sandy Cove
K25	697530	5496000	granite sill, highway north of Cobb Cove	Mafic dykes			
K28	699890	5497660	granite, dump west of Little Seldom	K61	700300	5498580	basalt dyke cutting microgranite, north of Little Seldom Cove
				K65	712140	5501750	basalt dyke cutting diorite complex, Western Head

UTM grid, zone 21, NAD 27 projection, NTS 1:50,000 sheet 2E/9 (Fogo), edition 3